Degassing of volcanic extrusives on Mercury: Potential contributions to transient atmospheres and buried polar deposits

Ariel N. Deutsch[1,2*], James W. Head[1], Stephen W. Parman[1], Lionel Wilson[1,3], Gregory A. Neumann[4], Finnian Lowden[1]

[1]Department of Earth, Environmental and Planetary Sciences, Brown University, Providence, RI 02912, USA

[2]Now at: NASA Ames Research Center, Mountain View, CA 94035, USA

[3]Lancaster Environment Centre, Lancaster University, Lancaster LA1 4YQ, UK

[4]NASA Goddard Space Flight Center, Greenbelt, MD 20771, USA

*Corresponding author: Ariel N. Deutsch

ariel_deutsch@brown.edu

Brown University

Box 1846, Providence, RI 02912

Date of draft: 8 February 2021

Keywords: Mercury, volcanism, polar deposits, atmospheres, Moon

Abstract

The surface of Mercury is dominated by extensive, widespread lava plains that formed early in its history. The emplacement of these lavas was accompanied by the release of magmatic volatiles, the bulk of which were lost to space via thermal escape and/or photodissociation. Here we consider the fate of these erupted volatiles by quantifying the volumes of erupted volcanic plains and estimating the associated masses of erupted volatiles. The concentrations and speciation of volatiles in Mercury's magmas are not known with certainty at this time, so we model a wide range of cases, based on existing experimental data and speciation models, at 3–7 log fO_2 units below conditions determined by the iron-wüstite buffer. Cases range from relatively low gas content scenarios (total exsolved gas mass of 9×10^{15} kg) to high gas content scenarios (total exsolved gas = 5×10^{19} kg). We estimate that the average duration of a transient volcanic atmosphere resulting from a single eruption would be between ~250 and ~210,000 years, depending on the volume, degassed volatile content, and eruption rate of an individual eruption, as well as the fO_2 conditions of the planet's interior. If a dense transient atmosphere was ever surface-bound long enough for the released volatiles to be transported to and cold-trapped at Mercury's polar regions, those trapped volatiles are predicted to be well-mixed with the regolith, and at least 16 m beneath the surface given regolith gardening rates. These volatiles would have a composition and age distinctly different from those of the H_2O-ice deposits observed at the poles of Mercury today.

Main text

1 Introduction

Discovering that Mercury is volatile-bearing is one of the most exciting findings of the MErcury Surface, Space ENvironment, GEochemistry, and Ranging (MESSENGER) mission given the planet's heliocentric distance. For example, Mercury has abundant and widely distributed pyroclastic deposits, indicative of volatile-rich eruptions (e.g., Head et al., 2009; Kerber et al., 2009; Thomas et al., 2014a, 2014b; Goudge et al., 2014; Jozwiak et al., 2018; Pajola et al., 2021). The size of these deposits suggests that they formed from an eruptive process that was even more volatile-rich than the process that formed lunar pyroclastic deposits (Kerber et al., 2009). Mercury also has intriguing hollows suggestive of sublimation, implying that abundant volatiles are present beneath the surface (Blewett et al., 2013). Additionally, MESSENGER X-Ray Spectrometer (XRS) and Gamma-Ray Spectrometer (GRS) measurements indicate the widespread and abundant presence of K, S, Na, and Cl, and that the planet is volatile-rich (e.g., Nittler et al. 2011; Peplowski et al. 2012, 2014; Evans et al. 2015).

Magmatism is a primary mechanism by which volatiles are transferred from the interiors of planets to the surface (e.g., Moore, 1970; Greeley, 1987). For example, laboratory analyses of Apollo samples revealed the presence of volatiles (H-, C-, S-, Cl-, and F-bearing compounds) trapped in primitive magmas (e.g., Saal et al., 2008), suggesting that lunar volcanism has effectively transferred volatiles from the interior to the surface of the Moon. As shown by the lunar volcanic record (e.g., Head and Wilson, 2017), basaltic volcanic eruptions can be of two types: effusive and explosive. Effusive eruptions involve the generation of mantle partial melts, their ascent toward the surface in magma-filled cracks (dikes) driven by buoyancy and overpressurization, and their eruption to the surface to form lava flows, accompanied by degassing at the vent (e.g., Wilson and Head, 2018). Needham and Kring (2017) estimated that ~10^{16} kg of CO and S and ~10^{14} kg of H_2O were released during the effusive formation of lunar lava plains (the maria), with the bulk of volatiles being released during peak mare emplacement at ~3.5 Gyr. The mare-erupted volatiles may have even been present in sufficient masses to produce a transient atmosphere (Needham and Kring, 2017), although the duration of and intervals between mare-forming eruptions have an important control on the density and lifetime of any volcanically-derived atmosphere (Head et al., 2020). Interestingly, the production of a substantially dense atmosphere would aid in the transport of volatiles to cold-trapping regions, and volcanically-derived volatiles have been predicted to be cold-trapped at the lunar poles today (e.g., Arnold, 1979; Crotts and Hummels, 2009; Needham and Kring, 2017).

Like the Moon, Mercury has been extensively resurfaced by large expanses of lava plains (Fig. 1) (Head et al., 2009, 2011; Denevi et al., 2013; Byrne et al., 2016, 2018). If effusive volcanism released substantial volatiles on the Moon during the production of the maria, it is possible that substantial volatiles were also released on Mercury during the production of volcanic plains, albeit with different chemical species and abundances (Nittler et al., 2011; Zolotov, 2011). Given the more widespread presence of pyroclastic deposits (Kerber et al., 2009; Thomas et al., 2014a, 2014b; Goudge et al., 2014; Jozwiak et al., 2018), and its generally higher volatile contents relative to the Moon, Mercury may be even more likely to have had a transient volcanically-derived atmosphere than the Moon. Here we seek to understand the magnitude and potential fate of erupted volatiles. We analyze the volume of volcanic plains on Mercury and estimate the amount of released gases, specifically for volatiles predicted to be indigenous to the planet. We then estimate the typical eruption frequency and associated released magma volumes and volatile masses. Finally, we discuss the potential fate of erupted volatiles and their relationship to volatiles observed in high-latitude cold traps on Mercury (e.g., Lawrence et al., 2013). The pre-eruptive volatile contents of Mercury's lavas are not well known, and existing experimental data do not constrain speciation well at mercurian igneous conditions (low oxygen fugacity, high S). Therefore, we examine a wide range of concentration and speciation cases in order to provide bounds on the amount of volatiles released during effusive eruptions.

2 Methods

2.1 Volume of erupted lavas on Mercury

Figure 1 shows the distribution of volcanic plains on Mercury. Smooth plains (SPs) are widely distributed across the planet and were originally suggested to be volcanic due to their tendency to embay other features and pond in topographic lows (e.g., Murray et al., 1974; Strom et al., 1975). Observations of these plains with MESSENGER later revealed a variety of volcanic landforms and morphologies (Head et al., 2009, 2011; Byrne et al., 2016; Denevi et al., 2013), and the SPs are interpreted to be from effusive, flood-mode eruptions (Head et al., 2009, 2011; Byrne et al., 2016, 2018). Denevi et al. (2013) found multiple lines of evidence (e.g., flooding and embayment relationships, color properties, and relationships with volcanic vents) indicating a volcanic origin for >65% of the SPs. As a conservative estimate, we assume in this study the total surface area of volcanic SPs (VSPs) to be 65% of the total mapped SPs surface area.

Figure 1 also delineates intercrater plains (ICPs), the most spatially dominant unit on Mercury. The ICPs are more heavily cratered than the SPs, suggesting they are relatively older

(Whitten et al., 2014). They were originally suggested to be volcanic because they occupy large volumes and because there is no obvious impact basin from which they may have been sourced as ejecta (e.g., Murray et al., 1974; Strom et al., 1975). The color properties of ICPs and SPs are similar (Murchie et al., 2015) and many of the contacts between these units exist as gradational boundaries (Whitten et al., 2014). These observations have led to the interpretation that ICPs are volcanic, emplaced in multiple, large-volume effusive flows (similar to the SPs), and have since been modified by impact cratering (Denevi et al., 2013; Whitten et al., 2014; Byrne et al., 2018). However, the origin of some ICPs is still debated and so we treat two different scenarios for estimating the total volume of effused lavas: first considering only VSPs and then also including the ICPs. In the models where ICPs are included, we assume that an additional ~40% of the planet's surface is covered by volcanically-derived ICPs.

For these two scenarios, we estimate the volume of plains by multiplying the surface area of each plains deposit by its estimated thickness, assuming VSPs are ~25% and volcanic ICPs are 40% of the planet's total surface area. Previous analyses indicate that the majority of volcanic plains on Mercury are between 0.5 km and 4 km thick (Byrne et al., 2018 and references therein). For plains that do not have previously resolved thicknesses, we estimate their thicknesses for three cases: (1) low volume (assuming a plains thickness, T, of 0.1 km), (2) intermediate volume (T =1 km), and (3) high volume (T=4 km).

In this analysis, we do not include the effect of explosively-formed pyroclastic deposits, which are relatively small and extend well into the post-regional plains part of Mercury's history (Thomas et al., 2014a, 2014b; Goudge et al., 2014; Jozwiak et al., 2018). Instead, we focus on the more widespread, and volumetrically-important, effusive volcanic plains.

2.2 Mercury's magmatic volatile content

We aim to provide upper and lower bounds for the amount of gas released on Mercury during extrusive plains-forming volcanism by exploring a wide parameter space of degassed contents and oxygen fugacities. In contrast to the Moon and Mars, we do not currently have any known samples of Mercury, which could help in the determination of its volatile content. In lieu of samples, XRS and GRS measurements of Mercury's surface and near-surface can provide some insight. These measurements - indicating abundances of K (Peplowski et al., 2012), C (Murchie et al., 2015), S (Nittler et al., 2011), Na (Peplowski et al., 2014), and Cl (Evans et al., 2015) - have been used widely in experiments and petrologic modeling to infer the melting conditions and mantle source compositions for surface lavas (e.g., Namur et al., 2016). The measurements of elevated S abundances (up to 4 wt. % at the surface; Nittler et al., 2011) also allow for the calculation of the planet's oxygen fugacity (fO_2), which is estimated to be between IW-3 and IW-7 (where IW-3 is 3 log units below the iron-wüstite oxygen buffer), indicating that Mercury is the most reduced terrestrial planet (Zolotov, 2011; Zolotov et al., 2013; Namur et al., 2016; McCubbin et al., 2017).

Our primary approach to estimating volcanic degassing rates uses experimentally-measured solubilities of volatiles at reducing conditions and at pressures relevant to mantle magma-generation regions (1–3 GPa). Thus, we are assuming that the melts are sourced from the mantle (90–270 km), and not crustal melting or direct impact heating. We use the melting pressures (rather than eruptive pressures), as this sets an upper limit to the amount of volatiles that can be mobilized by melting and delivered to the surface. Currently, there are no published experimental data that meet all of the desired criteria: data derived from experiments that vary

fO_2 values from IW-3 to IW-7, reproduce surface to mantle pressures appropriate to Mercury, include all volatiles (particularly S), and reproduce a major elemental composition similar to that of NSP and ICP lavas. Therefore, values in Table 1 are gathered from a range of experimental studies. These studies sometimes vary in magma composition and experimental conditions, and so are unfortunately not self-consistent (e.g., some values are from Fe-bearing melts, others are Fe-free; some melts have S, others do not). In some cases, the values had to be extrapolated to IW-7. The high-pressure solubilities set the maximum concentration of volatiles in magmas delivered to the surface, equivalent to assuming that the melts were volatile-saturated during melting and that there was no degassing during transport, as typically occurs on Earth. Both assumptions are not likely to be true, and so the actual concentrations in the pre-eruptive magmas are likely to be lower. We then estimate how much of those volatiles are actually degassed to the atmosphere, versus remaining in the lava as unexsolved volatiles, being trapped in vesicles, or being precipitated as solids. How much of the volatiles actually degasses depends on numerous factors, including how quickly the magmas ascend, how much they are oxidized (or reduced) by crustal interaction, how pressure affects solubility, and what solid phases would precipitate from the magma and/or condense from the volcanic gas. Since none of these factors are well constrained, we make very simple assumptions about the fraction of gas released to estimate high- and low-gas cases. These estimates are meant to place upper and lower bounds on degassing, but given the current state of knowledge, are unlikely to be accurate as to the exact composition or speciation of the degassed volatiles.

To supplement this approach, we also calculate degassing scenarios for specific cases of volatile speciation presented in Zolotov (2011) (Supporting Information). For 45/48 of these cases, the overall amounts of degassed volatiles fall within the range of our high- and low-gas models, though the details of the gas composition differ (Tables S1–S3). The major conclusions of our work do not change when using these different models.

At Mercury's reducing conditions, S has high concentrations and affects the partitioning and speciation of other volatiles in the melts (Zolotov, 2011; Zolotov et al., 2013; Armstrong et al., 2015; Namur et al., 2016; Anzures et al., 2020). Highly reducing conditions promote high S solubility via bonding with Ca, Mg, and Na in the melt structure, and this solubility has been measured in various experimental studies (e.g., McCoy et al., 1999; Namur et al., 2016; Anzures et al., 2020). At the high pressures (up to 4 GPa) and temperatures (1200–1750 °C) predicted for mercurian mantle conditions, S solubility in a sulfide-saturated experimental melt increases from ~1 wt. % to ~7 wt. % as fO_2 decreases from IW-3 to IW-7 (Namur et al., 2016). At present, how much of this S will degas from the magma is not known. A significant factor in this uncertainty is how much the lavas are oxidized (or reduced) as they transit the crust (Zolotov, 2011). Oxidation will greatly lower S solubility, and thus promote abundant S degassing. The high S that remains in the lavas, as measured by XRS, suggests that a significant amount of the dissolved S is trapped in sulfides, indicating limited (or lack of) crustal oxidation of the magma. We consider two cases: Model A, a low-gas scenario in which only 1% of the S content degasses (the rest forming sulfides), and Model B, a high-gas scenario in which 10% of the S content degasses. Given the uncertainties about Mercury's interior, our intention is to explore a broad parameter space with different models. Table 1 displays the various S contents explored here, and S content in the melts are assumed to be the experimentally-measured sulfur concentrations at sulfide saturation (SCSS). Note that in reality, volatile abundances are not simply determined by solubility limits, but also depend on bulk abundances. Our goal here is provide firm upper and lower bounds on the problem, and the solubility limits are a good upper bound.

For Mercury's interior, a major consideration is how elevated S abundances influence the melt, given that S saturation affects the bonding environment of other species, particularly in a low-O system. Measurements of sulfide-saturated experimental melts indicate that there is an increase in Cl solubility with decreasing fO_2 (e.g., Zolotov, 2011; Evans et al., 2015; Anzures et al., 2020). From these experiments, we estimate that Cl may be present in mercurian melts at abundances between 10 ppm and 800 ppm for fO_2 values between IW-3 and IW-7, respectively (Table 1). Again, it is not yet understood how much of any specific volatile species is released during eruptions on Mercury, so we estimate degassed contents for Cl (and all other non-S volatiles) as 10% for our low-gas Model A and 100% for our high-gas Model B.

C solubility has also been measured in various experimental studies. For example, Ardia et al. (2013) measured dissolved C in synthetic basaltic melts at pressures up to 3 GPa, temperatures between 1400 and 1450 °C, and fO_2 between IW-3 and IW-5. More recently, Dalou et al. (2019) measured dissolved C in reduced basaltic glasses at pressures up to 3 GPa and temperatures between 1400 and 1600 °C. Both studies provide similar estimates for dissolved C at IW-3 (100 ppm), which we use here (Table 1), although they do not explore lower fO_2 conditions. We estimate C at IW-7 as 10 ppm (Table 1) using the results of Armstrong et al. (2015), who experimentally studied (1.2 GPa, 1400 °C) the solubility and speciation of dissolved volatiles in mafic melts specifically for C-O-H-N species. Notably, the experiments of Armstrong et al. (2015) included the presence of H_2O, which is not predicted to be present in Mercury's interior (Nittler et al., 2011; Zolotov, 2011). The values used in our models (Table 1) reflect a decrease in C solubility with decreasing fO_2, but we note that recent experiments on sulfide-saturated systems suggest that C solubility increases with decreasing fO_2 (Anzures et al., 2020) and future work can help refine our models presented here.

Armstrong et al. (2015) also predicted dissolved N- and H-bearing melt species to be stable at high pressure and reducing conditions. N solubility was measured by Libourel et al. (2003) in S- and Fe-free basaltic melts at a range of fO_2 values between IW-1.3 and IW-8.3. We estimate the maximal possible N content for IW-3 and IW-7 from these experiments (Table 1). Maximal H contents at IW-3 are estimated from Dalou et al. (2019), and extrapolated down to IW-7 from Ardia et al. (2013) (Table 1).

Finally, we use estimates of C to estimate O content; assuming that all O in gas is present as CO or COS (Zolotov, 2011), we calculate the elemental abundance of O from the estimated moles of C released (Table 1).

We next estimate the total mass of volatiles delivered to the surface during the formation of volcanic plains on Mercury. We use the terms "delivered to the surface" and "released" to describe all of the volatiles that reach the surface, including both the volatiles that were outgassed to the atmosphere during initial dike penetration to the surface and hawaiian/strombolian pyroclastic activity and those that remain trapped in the solidified magma (e.g., vesicles, etc.) and diffuse out over much longer time scales (e.g., Wilson and Head, 2017, 2018). With our estimates of species released during mercurian eruptions (Table 1), we calculate the total mass of released volatiles, G, for each volcanic plains deposit from

$$G = V \times \rho_m \times n \qquad \text{(Eq. 1)},$$

where V is the total erupted volume, ρ_m is the bulk density of volcanic deposits on Mercury (~3014 kg m^{-3}; Padovan et al., 2015), and n is the estimated mass fraction of volatiles released from magmas delivered to the surface (Table 1).

We stress that Table 1 represents our estimates of the possible volatiles that were released during plains-forming eruptions on Mercury, but the actual volatile species and their degassed content remain unknown. We cannot emphasize enough that our approach is to bound the problem, and then present the different possibilities within these bounds. We examine a wide parameter space of degassed contents and oxygen fugacities in order to derive reasonable estimates for the amount of gas released on Mercury during plains-forming eruptions, and demonstrate how sensitive the models are to the gas content of the magmas. Future *in situ* analyses, as well as new experimental studies, are essential for more accurately describing the volatile speciation and content of mercurian lavas.

3 Results

3.1 Total volume of erupted lavas

The total volume of erupted lavas estimated for Mercury's VSPs ranges between ~1.1×10^7 and 4.6×10^7 km^3 depending on the estimated thicknesses of the plains (Fig. 2), equating to a global equivalent layer (GEL) of lava that is 0.15–0.61 km thick. The total amount of erupted lavas is likely to have been higher given that not all volcanic deposits are preserved at the surface today (Whitten et al., 2014). Assuming ICPs are also volcanic flows (Murray et al., 1974; Strom et al., 1975; Denevi et al., 2013; Whitten et al., 2014; Byrne et al., 2018), then the estimated volume of erupted lavas increases by up to an order of magnitude; the total erupted VSP and ICP volume is estimated to be ~1.4×10^7–1.7×10^8 km^3 (~0.19–2.3 km GEL) (Fig. 2).

Our conservative estimates of the total volume of erupted VSPs on Mercury are an order of magnitude higher than that most recently estimated for the Moon by Needham and Kring (~8.9×10^6 km^3; 0.23 km GEL), and similar to the ~10^7 km^3 (0.26 km GEL) estimated previously (Head and Wilson, 1992; Evans et al., 2016). The total volume of erupted lavas on Mercury is up to 2 orders of magnitude higher than that on the Moon if the ICPs are indeed volcanic. Overall, SP volcanism on Mercury appears to have largely begun to wane prior to ~3.5 Ga (Byrne et al., 2016; see Supporting Information), when mare volcanism may have been most active on the Moon (Hiesinger et al., 2011).

Uncertainties in the erupted volume stem from uncertainties associated with the estimates of volcanic plains thicknesses. While the thicknesses of some individual plains units have been resolved from stratigraphy (Byrne et al., 2018 and references therein), the thicknesses of others have not been analyzed in detail. Individual plains units are not predicted to be uniform in thickness; they vary in thickness as a function of eruption conditions, magmatic flux, viscosity, and geologic setting (Wilson and Head, 2008, 2017; Head et al., 2009, 2011; Denevi et al., 2013; Whitten and Head, 2013). To account for these uncertainties, as discussed in Section 2.1, we have computed the volume for three different volume scenarios.

3.2 Mass of erupted volatiles

We calculate the overall mass of degassed volatiles on Mercury (Table 2; Fig. 3) using estimates of total erupted lavas for the low-, intermediate-, and high-volume cases (Fig. 2). First we consider only the volatiles released during VSP-forming eruptions. Assuming an upper fO_2 of IW-3 in the intermediate-volume case, we estimate that ~2.0×10^{16} kg of volatiles were released during the formation of VSPs in a low-gas scenario (Model A), and ~2.0×10^{17} kg in a high-gas scenario (Model B). Assuming a lower fO_2 of IW-7 in the intermediate-volume case, we estimate that ~7.9×10^{17} kg of volatiles were released during the formation of SPs in Model A, and ~7.9 ×

10^{18} kg in Model B. Our estimates for S-, C-, H-, N-, Cl-, and O-bearing species are shown in Table 2.

If the ICPs are indeed volcanic, then the estimated masses of released volatiles would be even greater. For example, for the intermediate-volume case and an fO_2 of IW-3, ~4.5 × 10^{16} kg volatiles were released in Model A and ~4.5 × 10^{17} kg in Model B when including the contributions from both VSP-forming and ICP-forming eruptions. When assuming a lower fO_2 of IW-7, these estimates increase to ~1.8 × 10^{18} kg for Model A and ~1.8 × 10^{19} kg for Model B.

We also complete these calculations for specific mercurian degassing models presented by Zolotov (2011) in the Supporting Information. We find that the major conclusions presented here do not change when considering these specific models, given that our models are much more sensitive to the total amount of erupted gas as opposed to the specific species.

The difference in the abundance of released volatiles between Mercury and the Moon is largely a function of the total volume of erupted lavas, which is estimated to be greater on Mercury (Section 3.1). Overall, the large volumes of erupted lavas on the surface imply that the VSP-forming eruptions released at least ~9.3 × 10^{15} kg of volatiles over time, representing a conservative estimate under IW-3 conditions in Model A. While Model A represents a conservative low-gas scenario (Table 1), the mass of erupted volatiles would be lower for more undersaturated magmas.

4 The potential for volcanically-derived transient atmospheres

Although abundant volatiles are predicted to have been released during the formation of lava plains on Mercury (Fig. 3) and the Moon (Wilson and Head, 2018), the fate of such volatiles is an important open question. It has been proposed that large amounts of released volatiles on the Moon could have produced a transient atmosphere that aided in the transport of volatiles to cold-trapping regions (Needham and Kring, 2017). Critically, the possibility of such an atmosphere is dependent not only on volatile abundance and speciation, but also on degassing dynamics, eruption lifetimes, atmospheric gas dynamics, and atmospheric loss rates.

The Moon, for example, was very volcanically active between ~4 and 3.5 Ga on geologic timescales, but individual eruptions occurred on relatively short (~100 day) timescales (Wilson and Head, 2017, 2018), implying that there were significant periods of inactivity between eruptions. Head et al. (2020) estimated this repose time between average lunar eruptions to be ~13,000–40,000 years.

Here, we perform similar calculations for Mercury to solve for the average time interval between average eruptions, τ_i, from

$$\tau_i = \frac{\tau_T}{V_T/V_e} \qquad \text{(Eq. 2)},$$

where τ_T is the timespan of volcanic activity (estimated to be ~1 Gyr; Byrne et al., 2018), V_T is the total erupted volume of plains (estimated to be ~10^7 km^3 for VSPs and ~10^8 km^3 for VSPs + ICPs in Section 3.1), and V_e is the average volume of a single eruption (estimated to be ~200–400 km^3 from the heights and lateral extents of lobate flow fronts; Wilson and Head, 2008). If we assume that volcanic activity was relatively constant over τ_T, then τ_i is estimated to be between ~20,000 and 40,000 years for VSP-forming eruptions, but between ~2,000 and 4,000 years when also considering ICP-forming eruptions. As with the Moon, it is possible that the frequency of eruptions was higher at the start of τ_T and then decreased through time (see Supporting Information), given the thermal and magmatic evolution of the planet (e.g., Wilson and Head, 2008; 2017).

Released volatiles must remain in the atmosphere for sufficient durations in order to migrate and become cold-trapped before they are photochemically destroyed or lost to space (Section 5). In order to determine the average duration of volcanically-derived transient atmospheres on Mercury, we first calculate the average eruption duration, τ_e, from

$$\tau_e = \frac{V_e}{F_l} \qquad \text{(Eq. 3)},$$

where V_e the volume of erupted lava and F_l is the flux of erupted lava. For typical eruptions on Mercury, V_e is between 200 and 400 km^3 and F_l is between 10^3 and 10^7 m^3 s^{-1} (Wilson and Head, 2008); thus, τ_e is estimated to be between ~2,300 and 4,600 days for low-flux eruptions, and < 1 day for extremely high-flux eruptions (Table 3).

From τ_e, we calculate the flux of erupted gas, F_g, using

$$F_g = \frac{G}{\tau_e} \qquad \text{(Eq. 4)},$$

where G is the mass of gas released for an average eruption. While we estimate that the total mass of erupted volatiles on Mercury may be between ~10^{15} and 10^{19} kg (Section 3.2), it will of course be substantially less for individual eruptions. Wilson and Head (2008) estimated that the average volume of a single eruption is between ~200 and 400 km^3, which implies that the total gas released, G, for average mercurian eruptions is ~1.6×10^{11}–3.3×10^{12} kg assuming an fO_2 of IW-3 and ~6.5×10^{12}–1.3×10^{14} kg assuming an fO_2 of IW-7. With these values, F_g is estimated to be ~830–8.3×10^7 kg s^{-1} for IW-3, and ~33,000–3.3×10^9 kg s^{-1} for IW-7 (Table 3).

We next estimate the scale height, H, of a volcanically-derived atmosphere to be 15 km from

$$H = \frac{Q \times T}{m \times g} \qquad \text{(Eq. 5)},$$

where Q is the universal gas constant (8.314 J mol^{-1} K^{-1}), T is Mercury's mean surface temperature (~440 K), m is the mean molecular mass of erupted volatiles (~64.1 kg $kmol^{-1}$ assuming an S_2 atmosphere), and g is the gravitational acceleration at Mercury's surface (3.7 m s^{-2}). The scale height is dependent on temperature, and thus varies with location (latitude or time-of-day). For example, H is between ~4 and 25 km depending on whether the eruption occurred on the nightside or dayside, respectively, due to the large differences in diurnal surface temperature (ΔT≈600 K). The temperature may also vary during the eruption lifetime due to the greenhouse effect, or through geologic time due to changes in solar luminosity. Note that because of Mercury's greater surface gravity and a predicted S-based atmosphere (as opposed to a CO-H_2O dominated lunar atmosphere), H is less than the estimated H for a lunar volcanically-derived atmosphere (38 km; Head et al., 2020), which would also vary depending on the time and location of the eruption (ΔT≈300 K).

We use H (estimated from the mean surface temperature) to solve for the surface density of a volcanically-derived atmosphere, ρ_s, using

$$\rho_s = \frac{G}{4\,\pi\,R^2 \times H} \qquad \text{(Eq. 6)},$$

where R is the planet's radius (2440 km). For IW-3, ρ_s is estimated to be ~1.4×10^{-7}–2.9×10^{-6} kg m^{-3} and for IW-7, ρ_s is estimated to be ~5.6×10^{-6}–1.1×10^{-4} kg m^{-3} (Table 3).

The pressure of a collisionally-supported atmosphere, P_s, is calculated using

$$P_s = \rho_s \times \mathrm{g} \times H \qquad \text{(Eq. 7)}.$$

We estimate P_s to be ~0.01–0.2 Pa for IW-3 and ~0.3–6 Pa for IW-7 (Table 3), although this likely represents a maximum local surface pressure that quickly decays in time and space.

Finally, the flux of gas released during individual eruptions can be compared with the loss rate of gases from the atmosphere. We estimate the total duration of a volcanically-derived atmosphere, τ_d, from

$$\tau_d = \frac{G}{F_{esc}} \qquad \text{(Eq. 8).}$$

(Note, see Houghton (2002) for more details on Eqs. 5–8). To date, we know little about the rate of atmospheric escape, F_{esc}, on Mercury, although various estimates have been made for the Moon. For example, Vondrak (1974) estimated a thermal escape of 60 kg s^{-1}, and this value was adopted by both Needham and Kring (2017) and Head et al. (2020) when evaluating lifetimes of potential volcanically-derived transient atmospheres on the Moon. However, the thermal escape flux exponentially depends on molecular mass such that larger molecules escape more slowly (e.g., Tucker et al., 2021), and the molecular mass of the atmosphere was not considered by these groups. For a heavier S-based atmosphere and due to the higher gravity on Mercury, the escape rate would be smaller on Mercury than on the Moon. Tucker et al. (2021) found that thermal escape processes are less important in a collisional atmosphere, and sputtering and photodissociation dominate, calculating a mass loss rate of 17 kg s^{-1} for a CO collisional atmosphere. These processes may be stronger at Mercury due to its proximity to the Sun. In absence of Mercury-specific studies, these lunar-specific values provide a first-order approximation for our analysis, and we approximate F_{esc} as 20 kg s^{-1}. Solving for τ_d implies that a typical volcanically-derived atmosphere would decay within ~250–210,000 years (Table 3). Note that using an F_{esc} of 60 kg s^{-1} would decrease these estimates to ~85–69,000 years.

Above we estimated the average time between eruptions on Mercury, τ_i, to be ~20,000–40,000 years, although possibly as short as ~2,000–4,000 years if the ICPs (as volcanic origin) are included. Comparisons between τ_d and τ_i indicate the following:

1. If VSPs are the only volcanic plains on Mercury, then a transient volcanic atmosphere would likely have dissipated prior to a subsequent eruption (Fig. 4). It is possible that transient volcanic atmospheres co-existed in low fO_2 (IW-7) and high-gas (Model B) conditions given that the predicted lifetime of volcanically-derived atmospheres would have been longer (Fig. 4).
2. In the more likely case that ICPs, like the VSPs, are volcanic, the majority of our models suggest that the average duration of transient, volcanic atmospheres would have exceeded the average duration between individual eruptions, suggesting that the frequency of eruptions may have resulted in the combination of denser, longer-lived atmospheres (Fig. 4). Only for the low-gas, high fO_2 scenarios would this not be the case (Table 3).

These implications are depicted in Figure 4, where τ_d and τ_i are compared for low-volume scenarios (V_e=200 km^3).

The average surface pressure and density of transient atmospheres vary in each case and are highest for longer-lived atmospheres (Table 3). These properties are expected to decrease through time as an atmosphere decays, although may increase if individual eruptions overlap in time (denoted by the less transparent portions of plots in Figure 4). With the generation of a sufficiently dense atmosphere, the migration of volatiles is no longer governed by ballistic hopping, but instead by the collisions between molecules (Stewart et al., 2011; Prem et al., 2015). While such an atmosphere remains gravitationally bound, its lower layers are shielded from photodestruction (the primary loss mechanism for volatiles on airless bodies), allowing more time for molecules to reach permanent cold traps (Stewart et al., 2011; Prem et al., 2015). Determining the ultimate fate of volatiles in transiently dense atmospheres on nominally airless bodies requires detailed modeling that depends on eruption dynamics, atmospheric loss rates, gas dynamics, and compositional evolution in an atmosphere that is evolving on geologically rapid timescales (e.g., Prem et al., 2015, 2019). Such modeling will be an important next step in assessing how volcanic eruptions altered Mercury's atmospheric density and composition, and how the collisional dynamics of transiently dense atmospheres affected the transport and retention of interior volatiles on Mercury.

5 Buried volatiles at the poles of Mercury?

Needham and Kring (2017) point out that only a fraction of the predicted water released from mare formation (~10^{14} kg) is needed to account for all of the remotely sensed water at the lunar poles (~10^{11} kg), and if mare volcanism did deliver ice to the lunar poles, it is likely to be buried in the subsurface. We find that Mercury released even greater volumes of volcanic material over time than the Moon (Fig. 2), and therefore greater amounts of volatiles were likely released (Fig. 3). Is it possible that some fraction of erupted volatiles was deposited in polar cold traps on Mercury?

Interestingly, K, Na, and Cl appear to have higher concentrations in Mercury's northern terrain, and it is possible that these volatiles may be released from warmer, equatorial terrains and lost to space or redistributed to cooler terrains (Peplowski et al., 2012; Nittler et al., 2018). However, not all volatiles on Mercury appear to be spatially correlated with temperature, including S, which is concentrated at mid-equatorial latitudes (Weider et al., 2015; Nittler et al., 2018). The northern enhancements of K, Na, and Cl may instead be related to compositionally distinct magmas, as they show a general correlation with the large Northern SPs unit (Peplowski et al., 2015; Evans et al., 2015). However, if temperature-induced mobilization of volatiles has occurred on Mercury, then the northern concentrations of K, Na, or Cl may be examples of volatiles migrating to the poles, similar to what could have happened with outgassed species early on in mercurian history. A critical test of the competing origin hypotheses for the northern volatile anomalies will be BepiColombo (Benkhoff et al., 2010) measuring the abundance of K, Na, and Cl at the south polar region of Mercury, where there is no large volcanic plains unit comparable to the one seen at the north pole, but there is a similar thermal environment that would allow for the cold-trapping of volatiles.

In addition to K, Na, and Cl, there is an increase in H at Mercury's north polar region, where the detection of enhanced neutron suppression (Lawrence et al., 2013) and reflectance measurements (Neumann et al., 2013; Deutsch et al., 2017) are consistent with the presence of nearly pure H_2O deposits cold-trapped at the poles. These H-rich deposits have highly reflective radar properties that are also indicative of a nearly pure H_2O composition, with <5% silicates by volume (Butler et al., 1993). The ice deposits have not been covered by regolith gardening processes (Butler et al., 1993; Crider and Killen, 2005) and have distinct reflectance properties (Chabot et al., 2016), sharp geologic contacts (Chabot et al., 2016), and crater spatial densities (Deutsch et al., 2019) suggestive of geologically young ages <200 Myr (Crider and Killen, 2005; Lawrence et al., 2013; Deutsch et al., 2019).

The composition and age of these surface ice deposits indicate that they are not derived from volcanism. At mantle pressures and Mercury's extremely reducing conditions, H_2O is not predicted to be present in magmas (e.g., Nittler et al., 2011; Zolotov, 2011) and the very young surface ages of ice deposits (Deutsch et al., 2019) are inconsistent with the timing of Mercury's volcanic activity. The H_2O ices observed at the surface of the poles are more likely to have been delivered by an external, cometary impactor (e.g., Butler et al., 1993; Chabot et al., 2016; Ernst et al., 2018; Deutsch et al., 2019).

However, given our analysis here, it is important to consider the possibility that volatiles other than H_2O were released from Mercury's interior and contributed some fraction of materials to polar cold traps. These volatiles would be distinctly different from the H_2O polar deposits observed today, raising the question: Where would they be and how could they be identified?

Any volatiles that are deposited on the surface of Mercury (originating in the interior or externally delivered) must face the space weathering environment, including strong irradiation and thermal stresses (e.g., McCord and Clark, 1979; Domingue et al., 2014) and high-velocity impactors (e.g., Borin et al., 2009; Domingue et al., 2014). While the elevated elemental abundances of volatiles on Mercury (Nittler et al., 2011; Zolotov, 2011; Peplowski et al., 2011, 2012; Evans et al., 2012) suggest that perhaps the regolith is effective at trapping volatiles, the high temperatures of non-polar surfaces are a major limiting factor governing volatile sequestration and retention. If volatiles do succumb to sequestration in the polar region, they can subsequently be destroyed through impact vaporization and melting, but also preserved by ejecta.

If any individual, volcanically-derived atmosphere was sufficiently dense and long-lasting, then perhaps some fraction of volatiles migrated to and became cold-trapped at the poles before the atmosphere completely attenuated. We find that such atmospheres were probably uncommon, but may have been produced under certain extreme conditions (high eruption volume, high lava flux, low oxygen fugacity; Table 3). The location of an eruption also has some control over the distribution of migrated volatiles (Prem et al., 2015, 2019). While the Northern SPs (Fig. 1) coincide with today's polar cold traps, these cold traps largely post-date the formation of the SPs, so perhaps older south polar cold traps would provide a better record of volcanically-derived volatiles. If we assume that a layer of volcanically-derived volatiles was ever cold-trapped at Mercury's poles during one of these more extreme volcanic events, then we can use a regolith gardening rate to predict the depth at which they would be concentrated. For example, if volatiles were delivered 3.8 Ga (before major plains-forming volcanism began to wane), then the regolith gardening rate of ~0.43 cm Myr^{-1} derived by Crider and Killen (2005) suggests that the peak concentration of remnant volatiles would be at ~16 m in the subsurface today. We consider this to be a minimum estimate, given that the regolith gardening rate derived by Crider and Killen (2005) is for the recent past (<100 Ma) and the volcanism we analyze here was most active before ~3.5 Ga, when impact rates were much higher (e.g., Le Feuvre and Wieczorek, 2011). The volatiles would be well-mixed with the regolith and have a highly heterogeneous spatial distribution due to the stochastic impact gardening process (e.g., Crider and Killen, 2005).

The detection of volcanically-derived volatiles (distinct from impact-derived volatiles in composition) would provide important new insight into Mercury's volcanic history, interior geochemical conditions, and exospheric/atmospheric evolution. Indigenous volatiles well-mixed with the regolith at least 16 m below the surface would not have been detectable by MESSENGER, nor would it be with BepiColombo, given the sensing depths of each spacecraft's spectrometers. But future analyses of young crater ejecta might provide insight into the presence of buried volatiles. BepiColombo (Benkhoff et al., 2010) can also help refine many of the uncertainties associated with our current models. For example, analyses of plains morphometry can improve estimates of the volume of erupted lavas, and studying the morphology of the ICPs would be helpful in determining the extent to which they are volcanic. Higher-resolution images could also improve model production functions and thus the emplacement ages of plains units.

Furthermore, more detailed information on the numerous pyroclastic deposits and associated vents could increase our knowledge about whether they represent shallow concentrations of volatiles prior to eruption (Jozwiak et al., 2018), and how they compare to the effusive volcanic deposits documented here. Additional elemental measurements (particularly of S) can help refine geochemical models used to estimate the oxygen fugacity of Mercury's interior. Ultimately, sample analyses of Mercury's volcanic plains are needed to directly measure the speciation and volatile content of lavas (https://science.nasa.gov/science-red/s3fs-public/atoms/files/Mercury%20Lander.pdf).

6 Conclusion

Here we provide the first comprehensive estimates of the amounts of predicted volatiles (S, C, H, N, Cl, and O) released on Mercury via extrusive volcanic plains-forming eruptions using a variety of fO_2 conditions, degassing scenarios, and erupted volume estimates. We estimate that ~1.1–4.6 × 10^7 km^3 of lava erupted to form volcanic smooth plains (estimated here to be ~25% of the planet's total surface area), which is greater than the ~8.9 × 10^6 –1.0 × 10^7 km^3 of lava predicted for the lunar maria (Head and Wilson, 1992; Evans et al., 2016; Needham and Kring, 2017). A critical open question is the origin of Mercury's intercrater plains, which are the most spatially dominant geologic unit on the planet (Whitten et al., 2014). If an additional 40% of the surface area of Mercury is also volcanic (Murray et al., 1974; Strom et al., 1975; Denevi et al., 2013; Whitten et al., 2014; Byrne et al., 2018), then potentially up to 2 orders of magnitude more lavas were erupted to form volcanic plains on Mercury than erupted to form the lunar maria, over a similar length of time. The large volumes of erupted lavas on Mercury imply that large amounts of volatiles were released during the eruptive phases, which may have resulted in the transient production of enhanced atmospheric pressures with lifetimes between ~250 and ~210,000 years.

It is possible that these atmospheric lifetimes were greater than the time of repose between average mercurian eruptions (~20,000–40,000 years for SPs-forming eruptions or 2,000–4,000 years when also including ICPs-forming eruptions), creating dense, collisional transient atmospheres. Such atmospheres would enable more volatiles to migrate across the planet before they are photodestroyed and lost to space, increasing the probability of the erupted volatiles being cold-trapped (Stewart et al., 2011; Prem et al., 2015). For volatiles that did become cold-trapped at Mercury's poles, we estimate that they would be well-mixed with the regolith and at least ~16 m below the subsurface given regolith gardening rates (Crider and Killen, 2005). Such sequestered volatiles would be distinctly different from the polar H_2O-ice deposits observed on Mercury's surface today, both in composition (Butler et al., 1993; Lawrence et al., 2013) and in age (Crider and Killen, 2005; Lawrence et al., 2013; Deutsch et al., 2019).

Acknowledgements

We gratefully acknowledge the helpful reviews of this study by Mikhail Zolotov, Paul Byrne, and editor William McKinnon. This work was supported by NASA (Grant Number 80NSSC19K1289) issued through the Harriett G. Jenkins Graduate Fellowship to A. N. D., by the Solar System Exploration Research Virtual Institute (NNA14AB01A) to J. W. H., by the

Leverhulme Trust through an Emeritus Fellowship to L. W., and by NASA's Planetary Science Division Research Program to G. A. N.

References

Anzures, B.A., Parman, S.W., Milliken, R.E., Namur, O., Cartier, C., Wang, S., 2020. Effect of sulfur speciation on chemical and physical properties of very reduced mercurian melts. Geochimica et Cosmochimica Acta 286, 1–18. https://doi.org/10.1016/j.gca.2020.07.024

Ardia, P., Hirschmann, M.M., Withers, A.C., Stanley, B.D., 2013. Solubility of CH4 in a synthetic basaltic melt, with applications to atmosphere–magma ocean–core partitioning of volatiles and to the evolution of the Martian atmosphere. Geochimica et Cosmochimica Acta 114, 52–71. https://doi.org/10.1016/j.gca.2013.03.028

Armstrong, L.S., Hirschmann, M.M., Stanley, B.D., Falksen, E.G., Jacobsen, S.D., 2015. Speciation and solubility of reduced C–O–H–N volatiles in mafic melt: Implications for volcanism, atmospheric evolution, and deep volatile cycles in the terrestrial planets. Geochimica et Cosmochimica Acta 171, 283–302. https://doi.org/10.1016/j.gca.2015.07.007

Arnold, J.R., 1979. Ice in the lunar polar regions. J. Geophys. Res. 84, 5659–5668. https://doi.org/10.1029/JB084iB10p05659

Benkhoff, J., van Casteren, J., Hayakawa, H., Fujimoto, M., Laakso, H., Novara, M., Ferri, P., Middleton, H.R., Ziethe, R., 2010. BepiColombo—Comprehensive exploration of Mercury: Mission overview and science goals. Planetary and Space Science, Comprehensive Science Investigations of Mercury: The scientific goals of the joint ESA/JAXA mission BepiColombo 58, 2–20. https://doi.org/10.1016/j.pss.2009.09.020

Blewett, D.T., Vaughan, W.M., Xiao, Z., Chabot, N.L., Denevi, B.W., Ernst, C.M., Helbert, J., D'Amore, M., Maturilli, A., Head, J.W., Solomon, S.C., 2013. Mercury's hollows: Constraints on formation and composition from analysis of geological setting and spectral reflectance. Journal of Geophysical Research: Planets 118, 1013–1032. https://doi.org/10.1029/2012JE004174

Borin, P., Cremonese, G., Marzari, F., Bruno, M., Marchi, S., 2009. Statistical analysis of micrometeoroids flux on Mercury. Astronomy and Astrophysics 503, 259–264. https://doi.org/10.1051/0004-6361/200912080

Butler, B.J., 1997. The migration of volatiles on the surfaces of Mercury and the Moon. J. Geophys. Res. 102, 19283–19291. https://doi.org/10.1029/97JE01347

Byrne, P. K., Whitten, J. L., Klimczak, C., McCubbin, F. M., Ostrach, L. R., 2018. The volcanic character of Mercury. Mercury: The view after MESSENGER. Edited by Solomon S. C., Nittler, L. R., Anderson, B. J. Cambridge Univ. Press, pp. 287–323.

Byrne, P.K., Ostrach, L.R., Fassett, C.I., Chapman, C.R., Denevi, B.W., Evans, A.J., Klimczak, C., Banks, M.E., Head, J.W., Solomon, S.C., 2016. Widespread effusive volcanism on Mercury likely ended by about 3.5 Ga. Geophys. Res. Lett. 43, 2016GL069412. https://doi.org/10.1002/2016GL069412

Chabot, N.L., Ernst, C.M., Paige, D.A., Nair, H., Denevi, B.W., Blewett, D.T., Murchie, S.L., Deutsch, A.N., Head, J.W., Solomon, S.C., 2016. Imaging Mercury's polar deposits during MESSENGER's low-altitude campaign. Geophys. Res. Lett. 43, 9461–9468. https://doi.org/10.1002/2016GL070403

Crider, D., Killen, R.M., 2005. Burial rate of Mercury's polar volatile deposits. Geophys. Res. Lett. 32, L12201. https://doi.org/10.1029/2005GL022689

Crotts, A.P.S., Hummels, C., 2009. Lunar Outgassing, Transient Phenomena, and the Return to the Moon. II. Predictions and Tests for Outgassing/Regolith Interactions. ApJ 707, 1506. https://doi.org/10.1088/0004-637X/707/2/1506

Dalou, C., Hirschmann, M.M., Jacobsen, S.D., Le Losq, C., 2019. Raman spectroscopy study of C-O-H-N speciation in reduced basaltic glasses: Implications for reduced planetary mantles. Geochimica et Cosmochimica Acta 265, 32–47. https://doi.org/10.1016/j.gca.2019.08.029

Denevi, B.W., Ernst, C.M., Meyer, H.M., Robinson, M.S., Murchie, S.L., Whitten, J.L., Head, J.W., Watters, T.R., Solomon, S.C., Ostrach, L.R., Chapman, C.R., Byrne, P.K., Klimczak, C., Peplowski, P.N., 2013. The distribution and origin of smooth plains on Mercury. J. Geophys. Res. Planets 118, 891–907. https://doi.org/10.1002/jgre.20075

Deutsch, A.N., Head, J.W., Neumann, G.A., 2019. Age constraints of Mercury's polar deposits suggest recent delivery of ice. Earth and Planetary Science Letters 520, 26–33. https://doi.org/10.1016/j.epsl.2019.05.027

Deutsch, A.N., Neumann, G.A., Head, J.W., 2017. New evidence for surface water ice in small-scale cold traps and in three large craters at the north polar region of Mercury from the Mercury Laser Altimeter. Geophys. Res. Lett. 44, 9233–9241. https://doi.org/10.1002/2017GL074723

Domingue, D.L., Chapman, C.R., Killen, R.M., Zurbuchen, T.H., Gilbert, J.A., Sarantos, M., Benna, M., Slavin, J.A., Schriver, D., Trávníček, P.M., Orlando, T.M., Sprague, A.L., Blewett, D.T., Gillis-Davis, J.J., Feldman, W.C., Lawrence, D.J., Ho, G.C., Ebel, D.S., Nittler, L.R., Vilas, F., Pieters, C.M., Solomon, S.C., Johnson, C.L., Winslow, R.M., Helbert, J., Peplowski, P.N., Weider, S.Z., Mouawad, N., Izenberg, N.R., McClintock, W.E., 2014. Mercury's Weather-Beaten Surface: Understanding Mercury in the Context of Lunar and Asteroidal Space Weathering Studies. Space Sci Rev 181, 121–214. https://doi.org/10.1007/s11214-014-0039-5

Ernst, C.M., Chabot, N.L., Barnouin, O.S., 2018. Examining the Potential Contribution of the Hokusai Impact to Water Ice on Mercury. Journal of Geophysical Research: Planets 123, 2628–2646. https://doi.org/10.1029/2018JE005552

Evans, A.J., Soderblom, J.M., Andrews-Hanna, J.C., Solomon, S.C., Zuber, M.T., 2016. Identification of buried lunar impact craters from GRAIL data and implications for the nearside maria. Geophys. Res. Lett. 43, 2015GL067394. https://doi.org/10.1002/2015GL067394

Evans, L.G., Peplowski, P.N., McCubbin, F.M., McCoy, T.J., Nittler, L.R., Zolotov, M.Yu., Ebel, D.S., Lawrence, D.J., Starr, R.D., Weider, S.Z., Solomon, S.C., 2015. Chlorine on the surface of Mercury: MESSENGER gamma-ray measurements and implications for the planet's formation and evolution. Icarus 257, 417–427. https://doi.org/10.1016/j.icarus.2015.04.039

Goudge, T.A., Head, J.W., Kerber, L., Blewett, D.T., Denevi, B.W., Domingue, D.L., Gillis-Davis, J.J., Gwinner, K., Helbert, J., Holsclaw, G.M., Izenberg, N.R., Klima, R.L., McClintock, W.E., Murchie, S.L., Neumann, G.A., Smith, D.E., Strom, R.G., Xiao, Z., Zuber, M.T., Solomon, S.C., 2014. Global inventory and characterization of pyroclastic deposits on Mercury: New insights into pyroclastic activity from MESSENGER orbital data. Journal of Geophysical Research: Planets 119, 635–658. https://doi.org/10.1002/2013JE004480

Greeley, R., 1987. Release of Juvenile Water on Mars: Estimated Amounts and Timing Associated with Volcanism. Science 236, 1653–1654. https://doi.org/10.1126/science.236.4809.1653

Head, J.W., Chapman, C.R., Strom, R.G., Fassett, C.I., Denevi, B.W., Blewett, D.T., Ernst, C.M., Watters, T.R., Solomon, S.C., Murchie, S.L., Prockter, L.M., Chabot, N.L., Gillis-Davis, J.J., Whitten, J.L., Goudge, T.A., Baker, D.M.H., Hurwitz, D.M., Ostrach, L.R., Xiao, Z., Merline, W.J., Kerber, L., Dickson, J.L., Oberst, J., Byrne, P.K., Klimczak, C., Nittler, L.R., 2011. Flood Volcanism in the Northern High Latitudes of Mercury Revealed by MESSENGER. Science 333, 1853–1856. https://doi.org/10.1126/science.1211997

Head, J.W., Murchie, S.L., Prockter, L.M., Solomon, S.C., Chapman, C.R., Strom, R.G., Watters, T.R., Blewett, D.T., Gillis-Davis, J.J., Fassett, C.I., Dickson, J.L., Morgan, G.A., Kerber, L., 2009. Volcanism on Mercury: Evidence from the first MESSENGER flyby for extrusive and explosive activity and the volcanic origin of plains. Earth and Planetary Science Letters, MESSENGER's First Flyby of Mercury 285, 227–242. https://doi.org/10.1016/j.epsl.2009.03.007

Head, J.W., Wilson, L., 1992. Lunar mare volcanism: Stratigraphy, eruption conditions, and the evolution of secondary crusts. Geochimica et Cosmochimica Acta 56, 2155–2175. https://doi.org/10.1016/0016-7037(92)90183-J

Head, J.W., Wilson, L., 2017. Generation, ascent and eruption of magma on the Moon: New insights into source depths, magma supply, intrusions and effusive/explosive eruptions (Part 2: Predicted emplacement processes and observations). Icarus 283, 176–223. https://doi.org/10.1016/j.icarus.2016.05.031

Head, J.W., Wilson, L., Deutsch, A.N., Saal, A.E., Rutherford, M.L., Saal, A.E., 2020. Volcanically-induced transient atmospheres on the Moon: Assessment of duration, significance and contributions to polar volatile traps. Geophysical Research Letters 47, e2020GL089509. https://doi.org/10.1029/2020GL089509

Hiesinger, H., Head, J.W., Wolf, U., Jaumann, R., Neukum, G., 2011. Ages and stratigraphy of lunar mare basalts: A synthesis. Geological Society of America Special Papers 477, 1–51. https://doi.org/10.1130/2011.2477(01)

Houghton, J., 2002. The Physics of Atmospheres. Cambridge University Press, 3rd edition, 340 pp.

Jozwiak, L.M., Head, J.W., Wilson, L., 2018. Explosive volcanism on Mercury: Analysis of vent and deposit morphology and modes of eruption. Icarus 302, 191–212. https://doi.org/10.1016/j.icarus.2017.11.011

Kerber, L., Head, J.W., Solomon, S.C., Murchie, S.L., Blewett, D.T., Wilson, L., 2009. Explosive volcanic eruptions on Mercury: Eruption conditions, magma volatile content, and implications for interior volatile abundances. Earth and Planetary Science Letters, MESSENGER's First Flyby of Mercury 285, 263–271. https://doi.org/10.1016/j.epsl.2009.04.037

Lawrence, D.J., Feldman, W.C., Goldsten, J.O., Maurice, S., Peplowski, P.N., Anderson, B.J., Bazell, D., McNutt, R.L., Nittler, L.R., Prettyman, T.H., Rodgers, D.J., Solomon, S.C., Weider, S.Z., 2013. Evidence for Water Ice Near Mercury's North Pole from MESSENGER Neutron Spectrometer Measurements. Science 339, 292–296. https://doi.org/10.1126/science.1229953

Libourel, G., Marty, B., Humbert, F., 2003. Nitrogen solubility in basaltic melt. Part I. Effect of oxygen fugacity. Geochimica et Cosmochimica Acta 67, 4123–4135. https://doi.org/10.1016/S0016-7037(03)00259-X

McCord, T.B., Clark, R.N., 1979. The Mercury soil: Presence of Fe2+. Journal of Geophysical Research: Solid Earth 84, 7664–7668. https://doi.org/10.1029/JB084iB13p07664

McCoy, T.J., Dickinson, T.L., Lofgren, G.E., 1999. Partial melting of the Indarch (EH4) meteorite: A textural, chemical, and phase relations view of melting and melt migration. Meteoritics & Planetary Science 34, 735–746. https://doi.org/10.1111/j.1945-5100.1999.tb01386.x

McCubbin, F.M., Vander Kaaden, K.E., Peplowski, P.N., Bell, A.S., Nittler, L.R., Boyce, J.W., Evans, L.G., Keller, L.P., Elardo, S.M., McCoy, T.J., 2017. A Low O/Si Ratio on the Surface of Mercury: Evidence for Silicon Smelting? Journal of Geophysical Research: Planets 122, 2053–2076. https://doi.org/10.1002/2017JE005367

Moore, J.G., 1970. Water Content of Basalt Erupted on the ocean floor. Contr. Mineral. and Petrol. 28, 272–279. https://doi.org/10.1007/BF00388949

Murchie, S.L., Klima, R.L., Denevi, B.W., Ernst, C.M., Keller, M.R., Domingue, D.L., Blewett, D.T., Chabot, N.L., Hash, C.D., Malaret, E., Izenberg, N.R., Vilas, F., Nittler, L.R., Gillis-Davis, J.J., Head, J.W., Solomon, S.C., 2015. Orbital multispectral mapping of Mercury with the MESSENGER Mercury Dual Imaging System: Evidence for the origins of plains units and low-reflectance material. Icarus 254, 287–305. https://doi.org/10.1016/j.icarus.2015.03.027

Murray, B.C., Belton, M.J.S., Danielson, G.E., Davies, M.E., Gault, D.E., Hapke, B., O'Leary, B., Strom, R.G., Suomi, V., Trask, N., 1974. Mercury's Surface: Preliminary Description and Interpretation from Mariner 10 Pictures. Science 185, 169–179. https://doi.org/10.1126/science.185.4146.169

Namur, O., Charlier, B., Holtz, F., Cartier, C., McCammon, C., 2016. Sulfur solubility in reduced mafic silicate melts: Implications for the speciation and distribution of sulfur on Mercury. Earth and Planetary Science Letters 448, 102–114. https://doi.org/10.1016/j.epsl.2016.05.024

Needham, D.H., Kring, D.A., 2017. Lunar volcanism produced a transient atmosphere around the ancient Moon. Earth and Planetary Science Letters 478, 175–178. https://doi.org/10.1016/j.epsl.2017.09.002

Neumann, G.A., Cavanaugh, J.F., Sun, X., Mazarico, E.M., Smith, D.E., Zuber, M.T., Mao, D., Paige, D.A., Solomon, S.C., Ernst, C.M., Barnouin, O.S., 2013. Bright and dark polar deposits on Mercury: Evidence for surface volatiles. Science 339, 296–300. https://doi.org/10.1126/science.1229764

Nittler, L. R., Chabot, N. L., Grove, T. L., Peplowski, P. N., 2018. The chemical composition of Mercury. Mercury: The view after MESSENGER. Edited by Solomon S. C., Nittler, L. R., Anderson, B. J. Cambridge Univ. Press, pp. 20–51.

Nittler, L.R., Starr, R.D., Weider, S.Z., McCoy, T.J., Boynton, W.V., Ebel, D.S., Ernst, C.M., Evans, L.G., Goldsten, J.O., Hamara, D.K., Lawrence, D.J., McNutt, R.L., Schlemm, C.E., Solomon, S.C., Sprague, A.L., 2011. The Major-Element Composition of Mercury's Surface from MESSENGER X-ray Spectrometry. Science 333, 1847–1850. https://doi.org/10.1126/science.1211567

Padovan, S., Wieczorek, M.A., Margot, J.-L., Tosi, N., Solomon, S.C., 2015. Thickness of the crust of Mercury from geoid-to-topography ratios. Geophys. Res. Lett. 42, 2014GL062487. https://doi.org/10.1002/2014GL062487

Pajola, M., Lucchetti, A., Semenzato, A., Poggiali, G., Munaretto, G., Galluzzi, V., Marzo, G.A., Cremonese, G., Brucato, J.R., Palumbo, P., Massironi, M., 2021. Lermontov crater on Mercury: Geology, morphology and spectral properties of the coexisting hollows and pyroclastic deposits. Planetary and Space Science 195, 105136. https://doi.org/10.1016/j.pss.2020.105136

Peplowski, P.N., Evans, L.G., Stockstill-Cahill, K.R., Lawrence, D.J., Goldsten, J.O., McCoy, T.J., Nittler, L.R., Solomon, S.C., Sprague, A.L., Starr, R.D., Weider, S.Z., 2014. Enhanced sodium abundance in Mercury's north polar region revealed by the MESSENGER Gamma-Ray Spectrometer. Icarus 228, 86–95. https://doi.org/10.1016/j.icarus.2013.09.007

Peplowski, P.N., Lawrence, D.J., Rhodes, E.A., Sprague, A.L., McCoy, T.J., Denevi, B.W., Evans, L.G., Head, J.W., Nittler, L.R., Solomon, S.C., Stockstill- Cahill, K.R., Weider, S.Z., 2012. Variations in the abundances of potassium and thorium on the surface of Mercury: Results from the MESSENGER Gamma-Ray Spectrometer. Journal of Geophysical Research: Planets 117. https://doi.org/10.1029/2012JE004141

Prem, P., Artemieva, N.A., Goldstein, D.B., Varghese, P.L., Trafton, L.M., 2015. Transport of water in a transient impact-generated lunar atmosphere. Icarus, Lunar Volatiles 255, 148–158. https://doi.org/10.1016/j.icarus.2014.10.017

Prem, P., Goldstein, D.B., Varghese, P.L., Trafton, L.M., 2019. Coupled DSMC-Monte Carlo radiative transfer modeling of gas dynamics in a transient impact-generated lunar atmosphere. Icarus 326, 88–104. https://doi.org/10.1016/j.icarus.2019.02.036

Saal, A.E., Hauri, E.H., Cascio, M.L., Orman, J.A.V., Rutherford, M.C., Cooper, R.F., 2008. Volatile content of lunar volcanic glasses and the presence of water in the Moon's interior. Nature 454, 192–195. https://doi.org/10.1038/nature07047

Stewart, B.D., Pierazzo, E., Goldstein, D.B., Varghese, P.L., Trafton, L.M., 2011. Simulations of a comet impact on the Moon and associated ice deposition in polar cold traps. Icarus 215, 1–16. https://doi.org/10.1016/j.icarus.2011.03.014

Strom, R.G., Trask, N.J., Guest, J.E., 1975. Tectonism and volcanism on Mercury. Journal of Geophysical Research: Solid Earth 2478–2507. https://doi.org/10.1029/JB080i017p02478@10.1002/(ISSN)2169-9356.MERC1

Thomas, R.J., Rothery, D.A., Conway, S.J., Anand, M., 2014a. Long-lived explosive volcanism on Mercury. Geophysical Research Letters 41, 6084–6092. https://doi.org/10.1002/2014GL061224

Thomas, R.J., Rothery, D.A., Conway, S.J., Anand, M., 2014b. Mechanisms of explosive volcanism on Mercury: Implications from its global distribution and morphology. Journal of Geophysical Research: Planets 119, 2239–2254. https://doi.org/10.1002/2014JE004692

Tucker, O.J., Killen, R.M., Johnson, R.E., Saxena, P., 2021. Lifetime of a transient atmosphere produced by lunar volcanism. Icarus 359, 114304. https://doi.org/10.1016/j.icarus.2021.114304

Vondrak, R.R., 1974. Creation of an artificial lunar atmosphere. Nature 248, 657–659. https://doi.org/10.1038/248657a0

Whitten, J.L., Head, J.W., 2013. Detecting volcanic resurfacing of heavily cratered terrain: Flooding simulations on the Moon using Lunar Orbiter Laser Altimeter (LOLA) data. Planetary and Space Science 85, 24–37. https://doi.org/10.1016/j.pss.2013.05.013

Whitten, J.L., Head, J.W., Denevi, B.W., Solomon, S.C., 2014. Intercrater plains on Mercury: Insights into unit definition, characterization, and origin from MESSENGER datasets. Icarus 241, 97–113. https://doi.org/10.1016/j.icarus.2014.06.013

Wilson, L., Head, J.W., 2008. Volcanism on Mercury: A new model for the history of magma ascent and eruption. Geophysical Research Letters 35. https://doi.org/10.1029/2008GL035620

Wilson, L., Head, J.W., 2017. Generation, ascent and eruption of magma on the Moon: New insights into source depths, magma supply, intrusions and effusive/explosive eruptions (Part 1: Theory). Icarus, Lunar Reconnaissance Orbiter - Part II 283, 146–175. https://doi.org/10.1016/j.icarus.2015.12.039

Wilson, L., Head, J.W., 2018. Controls on lunar basaltic volcanic eruption structure and morphology: Gas release patterns in sequential eruption phases. Geophysical Research Letters 45, 5852–5859. https://doi.org/10.1029/2018GL078327

Zolotov, M.Yu., 2011. On the chemistry of mantle and magmatic volatiles on Mercury. Icarus 212, 24–41. https://doi.org/10.1016/j.icarus.2010.12.014

Zolotov, M.Yu., Sprague, A.L., Hauck, S.A., Nittler, L.R., Solomon, S.C., Weider, S.Z., 2013. The redox state, FeO content, and origin of sulfur-rich magmas on Mercury. J. Geophys. Res. Planets 118, 138–146. https://doi.org/10.1029/2012JE004274

Figures

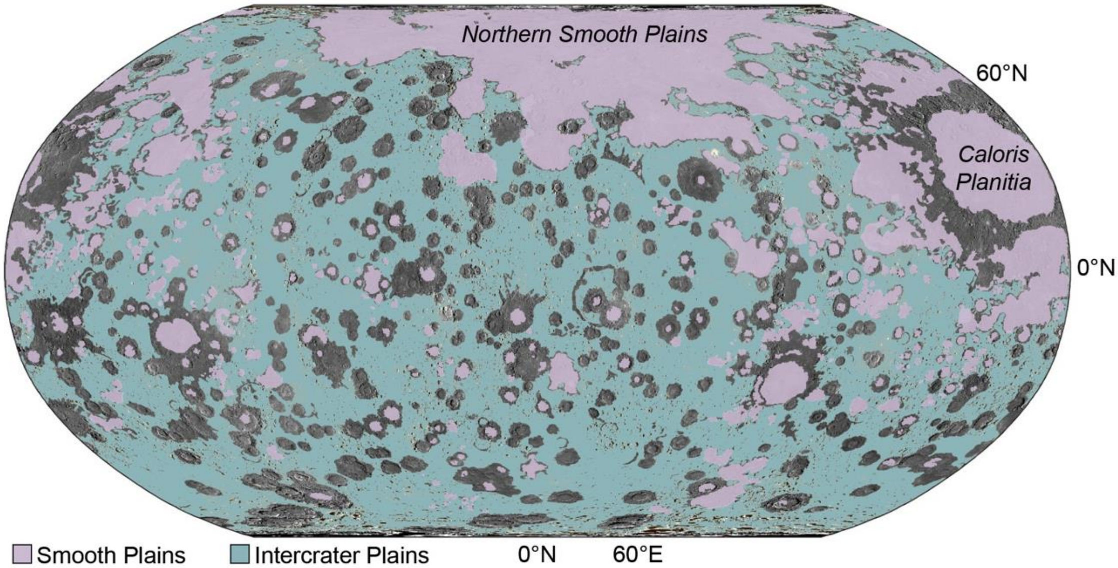

Fig. 1. The global distribution of smooth plains and intercrater plains on Mercury in Robinson projection (modified from Byrne et al., 2018).

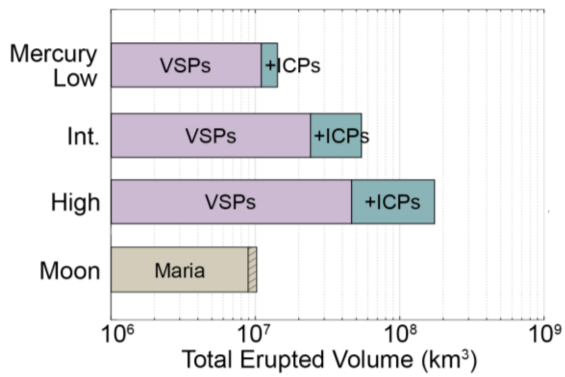

Fig. 2. Estimates of the total volume of erupted lavas on Mercury using low (0.1 km), intermediate (1 km), and high (4 km) estimates for previously unresolved plains thicknesses. These are compared with the predicted volume of erupted lavas on the Moon using the data from Needham and Kring (2017) as well as Head and Wilson (1992) and Evans et al. (2016) in hatching. Note that the volume is shown on a log scale.

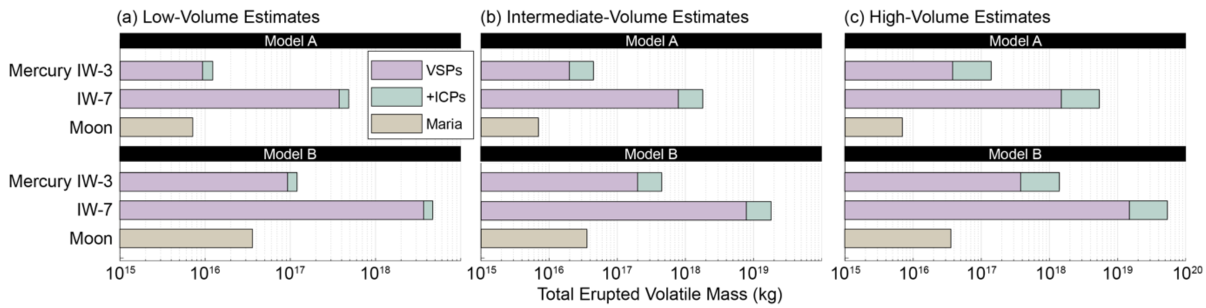

Fig. 3. Estimates of the total mass of volatiles released on Mercury from eruptions forming volcanic smooth plains (VSPs) and intercrater plains (ICPs), compared with the total mass of volatiles released during the formation of the maria estimated by Needham and Kring (2017). For fO_2 values of IW-3 and IW-7, estimates are computed for low-gas (Model A) and high-gas (Model B) scenarios. Recall, Model A estimates S abundances to be 1% SCSS and C-, H-, O-, N-, and Cl-abundances from 10% degassing amounts, while Model B estimates 10% of S and 100% of other volatiles degassed. We use a range of thicknesses (0.1, 1, and 4 km) for plains that lack previous estimates to derive (a) low-volume, (b) intermediate-volume, and (c) high-volume estimates. Note that the lunar estimates do not vary from (a) to (c), but do vary between low- and high-gas scenarios.

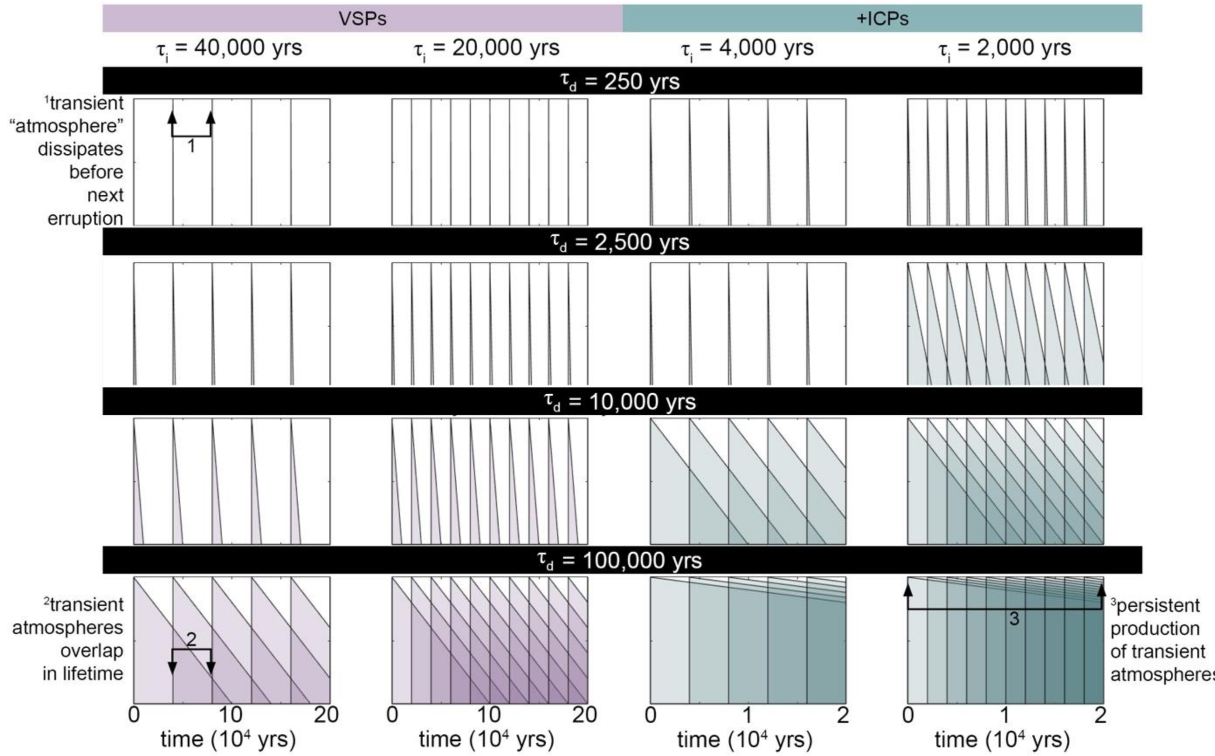

Fig. 4. Estimates of the total duration of volcanically-derived transient atmospheres from various model runs for low-volume scenarios (V_e=200 km^3; Table 3), where each triangular peak represents the formation of a volcanically-derived transient atmosphere, and the width of the triangle represents the duration of such an atmosphere. Although the individual eruptions are schematically represented as triangles, the decay of an eruption is not predicted to be linear. As the estimated time interval between average eruptions (τ_i) decreases across the columns, the intermittency spacing between eruptions decreases; eruptions are occurring every 40,000 years in the leftmost column and as frequently as every 2,000 years in the rightmost column. As the estimated duration of an average transient volcanically-derived atmosphere (τ_d) increases down the rows, the duration of a transient atmosphere increases; τ_d ranges from 250 to 2,500 years at IW-3 under degassing Models A and B, respectively, and from 10,000 to 100,000 years at IW-7

under Models A and B. Note that the x-axis is longer (200,000 years) in the first two columns than in the last two columns (20,000 years).

Tables

		Estimated Volatiles Delivered to the Surface							
		Mass, n (ppm)				Amount (wt. %)			
		IW-3		IW-7		IW-3		IW-7	
Element	Potential Degassing Species	Model A	Model B	Model A	Model B	Model A	Model B	Model A	Model B
S	S_2, S_3, CS_2, S_2Cl, COS, SCl_2	100	1,000	700	7,000	36	36	6	6
C	CO, CS_2, COS	10	100	1	10	3.6	3.6	0.01	0.01
H	H_2S, H_2, HCl	100	1,000	50	500	36	36	0	0
O	COS	13	133	1.3	13	4.9	4.9	0.01	0.01
N	N_2	50	500	10,000	100,000	18	18	92	92
Cl	Cl_2, S_2Cl, SCl_2, HCl, NaCl, $(NaCl)_2$, KCl	1	10	80	800	0.4	0.4	0.7	0.7

Table 1. Predicted volatile species for mercurian magmas. S abundances are estimated to be 1% of the estimated sulfur concentration at sulfide saturation (SCSS) for Model A and 10% of the estimated SCSS for Model B. Abundances of other elements are estimated from degassing amounts of 10% and 100% for Models A and B, respectively. Potential degassing species are discussed in detail by Zolotov (2011), Evans et al. (2015), Armstrong et al., (2015) and Dalou et al. (2019).

	Mass of Released Volatiles (kg)													
	S		C		H		N		Cl		O		Sum	
	Degassing Model													
	Model A (Low Gas)	Model B (High Gas)	Model A	Model B	Model A	Model B	Model A	Model B	Model A	Model B	Model A	Model B	Model A	Model B
	IW-3													
Volume Scenario	*Volcanic Smooth Plains Only*													
Low	3.4E+15	3.4E+16	3.4E+14	3.4E+15	3.4E+15	3.4E+16	1.7E+15	1.7E+16	3.4E+13	3.4E+14	4.4E+14	4.5E+15	9.3E+15	9.3E+16
Intermediate	7.3E+15	7.3E+16	7.3E+14	7.3E+15	7.3E+15	7.3E+16	3.6E+15	3.6E+16	7.3E+13	7.3E+14	9.5E+14	9.7E+15	2.0E+16	2.0E+17
High	1.4E+16	1.4E+17	1.4E+15	1.4E+16	1.4E+16	1.4E+17	7.0E+15	7.0E+16	1.4E+14	1.4E+15	1.8E+15	1.9E+16	3.8E+16	3.8E+17
	Volcanic Smooth Plains and Intercrater Plains													
Low	4.3E+15	4.3E+16	4.3E+14	4.3E+15	4.3E+15	4.3E+16	2.1E+15	2.1E+16	4.3E+13	4.3E+14	5.6E+14	5.7E+15	1.2E+16	1.2E+17
Intermediate	1.6E+16	1.6E+17	1.6E+15	1.6E+16	1.6E+16	1.6E+17	8.1E+15	8.1E+16	1.6E+14	1.6E+15	2.1E+15	2.2E+16	4.5E+16	4.5E+17
High	5.0E+16	5.0E+17	5.0E+15	5.0E+16	5.0E+16	5.0E+17	2.5E+16	2.5E+17	5.0E+14	5.0E+15	6.5E+15	6.6E+16	1.4E+17	1.4E+18
	IW-7													
	Volcanic Smooth Plains Only													
Low	2.4E+16	2.4E+17	3.4E+13	3.4E+14	1.7E+15	1.7E+16	3.4E+17	3.4E+18	2.7E+15	2.7E+16	4.4E+13	4.4E+14	3.7E+17	3.7E+18
Intermediate	5.1E+16	5.1E+17	7.3E+13	7.3E+14	3.6E+15	3.6E+16	7.3E+17	7.3E+18	5.8E+15	5.8E+16	9.5E+13	9.5E+14	7.9E+17	7.9E+18
High	9.8E+16	9.8E+17	1.4E+14	1.4E+15	7.0E+15	7.0E+16	1.4E+18	1.4E+19	1.1E+16	1.1E+17	1.8E+14	1.8E+15	1.5E+18	1.5E+19
	Volcanic Smooth Plains and Intercrater Plains													
Low	3.0E+16	3.0E+17	4.3E+13	4.3E+14	2.1E+15	2.1E+16	4.3E+17	4.3E+18	3.4E+15	3.4E+16	5.6E+13	5.6E+14	4.7E+17	4.7E+18
Intermediate	1.1E+17	1.1E+18	1.6E+14	1.6E+15	8.1E+15	8.1E+16	1.6E+18	1.6E+19	1.3E+16	1.3E+17	2.1E+14	2.1E+15	1.8E+18	1.8E+19
High	3.5E+17	3.5E+18	5.0E+14	5.0E+15	2.5E+16	2.5E+17	5.0E+18	5.0E+19	4.0E+16	4.0E+17	6.5E+14	6.5E+15	5.4E+18	5.4E+19

Table 2. Mass of erupted volatiles released during VSP- and ICP-forming eruptions estimated for fO_2 values of IW-3 and IW-7 and different degassing models. Model A represents a low-gas model where S abundances are estimated to be 1% of the estimated SCSS and abundances of other elements are estimated from degassing amounts of 10%. Model B is a high-gas model where 10% of S and

100% of other volatiles are estimated to have degassed. For each case, we present the low-, intermediate-, and high-volume estimates corresponding to different estimates of plains thicknesses (0.1, 1, and 4 km, respectively, for plains with previously unresolved thicknesses).

	V_e (km^3)	fO_2	Degassing Model	G (kg)	F_l (m^3 s^{-1})	τ_e (days)	F_g (kg s^{-1})	ρ_s (kg m^{-3})	P_s (Pa)	τ_d (years)
Low-Flux Scenario										
Low-Volume Scenario	200	IW-3	A	1.6×10^{11}	10^3	2,300	800	1.4×10^{-7}	0.008	250
			B	1.6×10^{12}			8,000	1.4×10^{-6}	0.08	2,500
		IW-7	A	6.5×10^{12}			33,000	5.6×10^{-6}	0.32	10,000
			B	6.5×10^{13}			330,000	5.6×10^{-5}	3.2	100,000
High-Volume Scenario	400	IW-3	A	3.3×10^{11}		4,600	830	2.9×10^{-7}	0.016	520
			B	3.3×10^{12}			8,300	2.9×10^{-6}	0.16	5,200
		IW-7	A	1.3×10^{13}			33,000	1.1×10^{-5}	0.64	21,000
			B	1.3×10^{14}			330,000	1.1×10^{-4}	6.4	210,000
High-Flux Scenario										
Low-Volume Scenario	200	IW-3	A	1.6×10^{11}	10^7	0.23	8.0×10^6	1.4×10^{-7}	0.008	250
			B	1.6×10^{12}			8.0×10^7	1.4×10^{-6}	0.08	2,500
		IW-7	A	6.5×10^{12}			3.3×10^8	5.6×10^{-6}	0.32	10,000
			B	6.5×10^{13}			3.3×10^9	5.6×10^{-5}	3.2	100,000
High-Volume Scenario	400	IW-3	A	3.3×10^{11}		0.46	8.3×10^6	2.9×10^{-7}	0.016	520
			B	3.3×10^{12}			8.3×10^7	2.9×10^{-6}	0.16	5,200
		IW-7	A	1.3×10^{13}			3.3×10^8	1.1×10^{-5}	0.64	21,000
			B	1.3×10^{14}			3.3×10^9	1.1×10^{-4}	6.4	210,000

Table 3. Predicted values to describe mercurian eruptions and resulting volcanically-derived atmospheres, including average volume of a single eruption (V_e), oxygen fugacity (fO_2), mass of total erupted gas (G), eruption rate (F_l), eruption duration (τ_e), gas release rate (F_g), transient atmospheric surface density (ρ_s), transient atmospheric surface pressure (P_s), and transient atmosphere duration (τ_d).